Vectorial Wave Analysis of Uniform-Core Optical Fibers Using a Novel Boundary Integral Method

NAOTO KISHI, MEMBER, IEEE, AND TAKANORI OKOSHI, FELLOW, IEEE

Abstract —**Vectorial wave analyses of uniform-core optical fibers using a novel boundary integral method that does not use Green's function, are presented. The expansion of the electromagnetic field on the boundary, the selection of the weight function, and the method for giving boundary conditions are discussed first. By using the formulation obtained, the propagation characteristics of elliptical-core optical fibers are analyzed. The effect of the boundary shape on the numerical results is also investigated through analyses of rectangular-core fibers. It is found that the new boundary integral method can easily be applied to solve vectorial wave boundary value problems.**

I. Introduction

IN A PREVIOUS paper [1], we proposed a new integral equation method called the boundary-integral method without using Green's function. This method has been found to be an efficient tool for solving Dirichlet- and Neumann-type boundary value problems of two-dimensional scalar wave equations. In the same report, we also suggested the possibility of using this method to solve general electromagnetic boundary value problems, such as the vectorial wave analysis of optical fibers.

The conventional boundary element method (BEM) [2]–[5] has been applied to the vectorial wave analyses of optical fibers [5]. However, in the BEM, the use of the Green's function not only is unnecessary but is also difficult because singularities exist in the function to be integrated [1]. What is more, the selection of the function on the boundary is difficult for the case of vectorial wave analyses.

To eliminate the singularities in the integration, the extended boundary condition method has been used [6], [7]. However, the formulation of that method is rather complicated.

In this paper, the new method is applied to the vectorial wave analysis of uniform-core optical fibers. This integral equation method has been proposed for eliminating the above difficulties in the conventional BEM. To be more specific, the weight functions which satisfy the Helmholtz equation are used in the new method instead of the Green's function in the conventional BEM. The electromagnetic functions on the boundary are expanded in Fourier series on a curvilinear coordinate. The validity of the formulation is proved by deriving the eigenvalue equations of a circular-core step-index optical fiber and comparing these with analytical solutions.

In the numerical analyses, consideration is given mainly to the propagation characteristics of elliptical-core optical fibers. The results show good agreement with the analytical solutions of Yeh [8]. The effect of the boundary shape on the numerical results is also investigated through analyses of rectangular-core fibers.

Manuscript received December 28, 1987; revised September 9, 1988.

N. Kishi is with the Department of Electronic Engineering, University of Electro-Communications, 1-5-1 Chofugaoka, Chofu-shi, Tokyo 182, Japan.

T. Okoshi is with the Research Center for Advanced Science and Technology (RCAST), University of Tokyo, 4-6-1 Komaba, Meguro-ku, Tokyo 153, Japan.

IEEE Log Number 8825383.

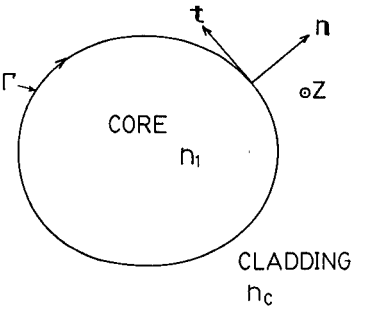

Fig. 1. Cross section of an arbitrarily shaped optical fiber core.

II. Basic Equations

We consider an optical fiber having an arbitrarily shaped core, whose cross section is shown in Fig. 1. It is assumed that in each region the material is homogeneous, isotropic, lossless, and nonmagnetic and that the cladding region extends to infinity. We denote the core and cladding regions by the subscripts 1 and C, respectively. Therefore, the z components of the electromagnetic field, E_z and H_z, satisfy the following Helmholtz equation in each region [9]:

$$\nabla_t^2 \begin{Bmatrix} E_{zi} \\ H_{zi} \end{Bmatrix} + \left(n_i^2 k_0^2 - \beta^2\right) \begin{Bmatrix} E_{zi} \\ H_{zi} \end{Bmatrix} = 0 \tag{1}$$

where $i = 1, C$ and

k_0 wavenumber of free space ($= \omega\sqrt{\epsilon_0 \mu_0}$),
n_i refractive index of each region,
β propagation constant of the propagation mode.

0018-9480/89/0300-0526$01.00 ©1989 IEEE

The transverse field components are derived from the z components as [9]

$$\boldsymbol{E}_{tl} = \frac{j\beta}{\beta^2 - n_i^2 k_0^2}\left(\nabla_t E_{zl} - \frac{\omega\mu_0}{\beta}\boldsymbol{a}_z \times \nabla_t H_{zl}\right) \tag{2a}$$

$$\boldsymbol{H}_{tl} = \frac{j\beta}{\beta^2 - n_i^2 k_0^2}\left(\nabla_t H_{zl} + \frac{\omega\epsilon_0 n_i^2}{\beta}\boldsymbol{a}_z \times \nabla_t E_{zl}\right). \tag{2b}$$

The boundary conditions on the core–cladding interface Γ are written as follows:

$$E_{z1} = E_{zC} \tag{3a}$$

$$H_{z1} = H_{zC} \tag{3b}$$

$$\boldsymbol{t}\cdot\boldsymbol{E}_{t1} = \boldsymbol{t}\cdot\boldsymbol{E}_{tC} \tag{3c}$$

$$\boldsymbol{t}\cdot\boldsymbol{H}_{t1} = \boldsymbol{t}\cdot\boldsymbol{H}_{tC} \tag{3d}$$

where

$$\boldsymbol{t}\cdot\boldsymbol{E}_{tl} = \frac{j\beta}{\beta^2 - n_i^2 k_0^2}\left(\frac{\partial E_{zl}}{\partial t} - \frac{\omega\mu_0}{\beta}\frac{\partial H_{zl}}{\partial n}\right) \tag{4a}$$

$$\boldsymbol{t}\cdot\boldsymbol{H}_{tl} = \frac{j\beta}{\beta^2 - n_i^2 k_0^2}\left(\frac{\partial H_{zl}}{\partial t} + \frac{\omega\epsilon_0 n_i^2}{\beta}\frac{\partial E_{zl}}{\partial n}\right). \tag{4b}$$

The tangential and normal unit vectors used in these equations, $\boldsymbol{t}$ and $\boldsymbol{n}$, are shown in Fig. 1.

III. Boundary Integral Formulation

To solve the boundary value problem of (1) and (3), the following boundary integral equation is used [1]:

$$\oint_\Gamma \left(\psi\frac{\partial\phi}{\partial n} - \phi\frac{\partial\psi}{\partial n}\right) dl = 0 \tag{5}$$

where ϕ stands for E_z or H_z and $(\partial\phi/\partial n)$ denotes its normal derivative on the boundary; ψ denotes a weight function [1] which satisfies (1) as E_z and H_z do.

In the following, we show (a) expressions for electromagnetic variables on the boundary Γ, (b) selection of the weight functions ψ, and (c) the matrix equation for the eigenvalues and eigenfunctions.

A. Electromagnetic Variables on the Boundary

In the previous paper, which dealt with single-potential problems [1], the field variables on the boundary Γ and their normal derivatives were expressed, as in the conventional BEM [2]–[5], by piecewise-linear functions as shown in Fig. 2(a). A higher order interpolation function [3] has also been used. However, in the case of hybrid-potential problems (problems for obtaining hybrid modes of propagation), the use of such functions on the boundary becomes difficult, as seen in the following.

When we apply the boundary conditions given by (3), we must calculate the tangential derivatives of E_z and H_z, which are the first terms on the right-hand sides of eqs. (4). These tangential derivatives $(\partial E_z/\partial t)$ and $(\partial H_z/\partial t)$ have an order lower by one than that of E_z and H_z (or the normal derivatives $(\partial E_z/\partial n)$ and $(\partial H_z/\partial n)$), as shown in Fig. 2(b); i.e., when the latter is piecewise linear, the former becomes discontinuous. Hence the right-hand sides of eqs. (4) will contain variables having different orders, which make the application of the boundary conditions difficult. In addition, the approximation of the boundary shape by straight line segments (called elements in the BEM analysis) reduces the numerical accuracy [1].

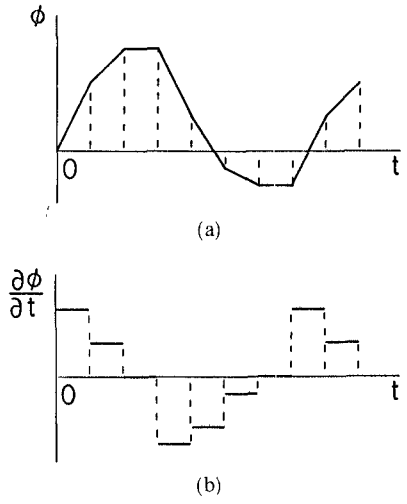

Fig. 2. Piecewise-linear function on the boundary in the conventional BEM [3]–[5]. (a) ϕ or its normal derivative $(\partial\phi/\partial n)$. (b) Tangential derivative $(\partial\phi/\partial t)$.

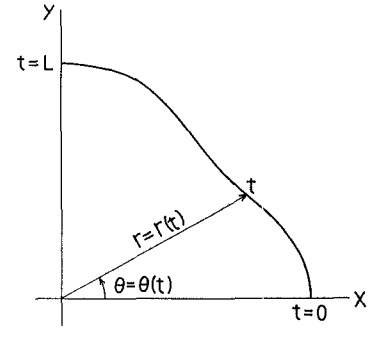

Fig. 3. Curvilinear coordinate t along the boundary for expression of field variables and cylindrical coordinate for expression of weight functions.

To overcome the above difficulties, we use here the curvilinear coordinate t along the boundary Γ, as shown in Fig. 3. When the boundary shape has symmetries with respect to the x and y axes, the field variables on the boundary also have such symmetries and are expanded in Fourier series as

$$E_z = \sum_j a_j \cos\left(\frac{j\pi t}{2L} + \rho\right) \tag{6a}$$

$$H_z = \sum_j b_j \sin\left(\frac{j\pi t}{2L} + \rho\right) \tag{6b}$$

$$\frac{\partial E_z^i}{\partial n} = \sum_j c_j^i \cos\left(\frac{j\pi t}{2L} + \rho\right) \tag{6c}$$

$$\frac{\partial H_z^i}{\partial n} = \sum_j d_j^i \sin\left(\frac{j\pi t}{2L} + \rho\right) \tag{6d}$$

where the superscript i $(=1, C)$ denotes the core and cladding regions, respectively, and L denotes the length of the boundary in the first quadrant. By using eqs. (6), the boundary conditions are easily applied in the spatial frequency region.

B. Weight Functions

We choose circular harmonics as the weight function ψ in the cylindrical coordinate; in other words, we use products of a Bessel function and a trigonometric function, as in the previous paper [1]. We should note that ψ will have different forms depending upon the function ϕ.

The weight functions in the core region are

$$\psi = J_n(\chi_1 r)\cos(n\theta + \rho) \quad \text{(for electric field)} \tag{7a}$$

$$\psi = J_n(\chi_1 r)\sin(n\theta + \rho) \quad \text{(for magnetic field)} \tag{7b}$$

$$\chi_1 = \left(n_1^2 k_0^2 - \beta^2\right)^{1/2} \tag{7c}$$

where $J_n(x)$ denotes the nth-order Bessel function of the first kind.

The weight functions in the cladding region are

$$\psi = K_n(\chi_C r)\cos(n\theta + \rho) \quad \text{(for electric field)} \tag{8a}$$

$$\psi = K_n(\chi_C r)\sin(n\theta + \rho) \quad \text{(for magnetic field)} \tag{8b}$$

$$\chi_C = \left(\beta^2 - n_C^2 k_0^2\right)^{1/2} \tag{8c}$$

where $K_n(x)$ denotes the nth-order modified Bessel function of the second kind.

C. Matrix Equation for Eigenvalue and Eigenfunction

We can now solve (5) using the above field variables and corresponding weight functions. Taking advantage of the symmetry of boundary conditions and field variables, we can restrict the contour integral of (5) to the first quadrant, selecting the orders n, j and rotation angle ρ as shown in Table I [1]. The number of weight functions is equal to that of the Fourier expansion coefficients of the corresponding mode. Thus, (5) can be rewritten as

$$[A^i]\boldsymbol{a} = [C^i]\boldsymbol{c}^i \tag{9a}$$

$$[B^i]\boldsymbol{b} = [D^i]\boldsymbol{d}^i \qquad (i=1,C) \tag{9b}$$

or

$$\boldsymbol{c}^i = [C^i]^{-1}[A^i]\boldsymbol{a} \tag{10a}$$

$$\boldsymbol{d}^i = [D^i]^{-1}[B^i]\boldsymbol{b} \qquad (i=1,C) \tag{10b}$$

where $[A^i],[B^i],[C^i],[D^i]$ $(i=1,C)$ are square matrices having the order same as the number of Fourier expansion coefficients of the corresponding field; $\boldsymbol{a}$ and $\boldsymbol{b}$ are numerical vectors consisting of the Fourier expansion coefficients of E_z and H_z, respectively; and $\boldsymbol{c}^i, \boldsymbol{d}^i$ $(i=1,C)$ are numerical vectors consisting of the Fourier expansion coefficients of $(\partial E_z/\partial n)$ and $(\partial H_z/\partial n)$, respectively. Equations (9) and (10) relate the fields on the boundary to their normal derivatives.

On the other hand, the tangential derivatives in (4a) and (4b) are easily obtained by differentiating (6a) and (6b).

TABLE I
SELECTION OF THE ORDER n, j AND ROTATION ANGLE ρ OF THE FIELD OR WEIGHT FUNCTION ψ ACCORDING TO THE SYMMETRY OF THE BOUNDARY CONDITIONS AND FIELD VARIABLES

symmetry of E_z about x- or y-axis		order and rotation angle	
x-axis	*y-axis*	n, j	ρ
symmetric	*symmetric*	*even*	0
symmetric	*antisymmetric*	*odd*	0
antisymmetric	*symmetric*	*odd*	$\pi/2$
antisymmetric	*antisymmetric*	*even*	$\pi/2$

Hence, all the terms on the right-hand sides of eqs. (4) can be expressed in terms of the Fourier coefficient vectors $\boldsymbol{a}$ and $\boldsymbol{b}$. Thus the boundary conditions (eq. (3)) can be applied. Note that the boundary conditions given by (3a) and (3b) are satisfied automatically, because E_z and H_z on the boundary, i.e., $\boldsymbol{a}$ and $\boldsymbol{b}$, are unknown variables.

Therefore, the matrix type eigenequation is given finally in the form

$$[M]\begin{bmatrix}\boldsymbol{a}\\ \boldsymbol{b}\end{bmatrix} = 0 \tag{11}$$

where $[M]$ denotes the square matrix having an order equal to the sum of the numbers of terms in the Fourier expansions for electric and magnetic fields.

The eigenvalue equation is obtained from (11) as

$$\det[M] = 0. \tag{12}$$

We can further calculate E_z and H_z by using (11), and hence $(\partial E_z/\partial n)$ and $(\partial H_z/\partial n)$ by means of (10).

IV. Eigenvalue Equation for Circular Step-Index Optical Fiber

To prove the validity of the formulation, we derive in this section the eigenvalue equation for a circular step-index optical fiber having a core radius a from the formulation given in the previous section.

In the previous section, field variables and weight functions have been selected according to the symmetry of eigenmodes. In this section, for simplicity we do not make such selections and perform the integration in (5) over all four quadrants. Because of the orthogonality of trigonometric functions, eqs. (10) become

$$\begin{bmatrix}\boldsymbol{c}^1\\ \boldsymbol{d}^1\end{bmatrix} = \operatorname{diag}\left[\frac{\chi_1 J_0'(\chi_1 a)}{J_0(\chi_1 a)}, \frac{\chi_1 J_1'(\chi_1 a)}{J_1(\chi_1 a)}, \cdots\right]\begin{bmatrix}\boldsymbol{a}\\ \boldsymbol{b}\end{bmatrix} \tag{13a}$$

$$\begin{bmatrix}\boldsymbol{c}^C\\ \boldsymbol{d}^C\end{bmatrix} = \operatorname{diag}\left[\frac{\chi_c k_0'(\chi_c a)}{k_0(\chi_c a)}, \frac{\chi_c k_1'(\chi_c a)}{k_1(\chi_c a)}, \cdots\right]\begin{bmatrix}\boldsymbol{a}\\ \boldsymbol{b}\end{bmatrix} \tag{13b}$$

where diag[$\cdots$] denotes a diagonal matrix.

Using eqs. (13) and the relations

$$\frac{\partial E_z}{\partial t} = -\sum_j \frac{j}{a} a_j \sin\left(\frac{jt}{a} + \rho\right) \tag{14a}$$

$$\frac{\partial H_z}{\partial t} = \sum_j \frac{j}{a} b_j \cos\left(\frac{jt}{a} + \rho\right) \tag{14b}$$

we can rewrite eqs. (11) as

$$-\frac{\beta}{\chi_1^2}\sum_j \left\{-\frac{j}{a}a_j - \frac{\omega\mu_0}{\beta}\cdot\frac{\chi_1 J_j'(\chi_1 a)}{J_j(\chi_1 a)} b_j\right\} \sin\left(\frac{jt}{a}+\rho\right)$$

$$= \frac{\beta}{\chi_c^2}\sum_j \left\{-\frac{j}{a}a_j - \frac{\omega\mu_0}{\beta}\cdot\frac{\chi_c k_j'(\chi_c a)}{k_j(\chi_c a)} b_j\right\} \sin\left(\frac{jt}{a}+\rho\right) \tag{15a}$$

$$-\frac{\beta}{\chi_1^2}\sum_j \left\{\frac{j}{a}b_j + \frac{\omega\epsilon_0 n_1^2}{\beta}\cdot\frac{\chi_1 J_j'(\chi_1 a)}{J_j(\chi_1 a)} a_j\right\} \cos\left(\frac{jt}{a}+\rho\right)$$

$$= \frac{\beta}{\chi_c^2}\sum_j \left\{\frac{j}{a}b_j + \frac{\omega\epsilon_0 n_c^2}{\beta}\cdot\frac{\chi_c k_j'(\chi_c a)}{k_j(\chi_c a)} a_j\right\} \cos\left(\frac{jt}{a}+\rho\right) \tag{15b}$$

to obtain finally

$$\begin{bmatrix} M_0 & 0 & & & & & \\ 0 & M_0' & & & & & \\ & & [M_1] & & 0 & & \\ & & & [M_2] & & & \\ & & & & \ddots & & \\ & & & & & [M_j] & \\ & & 0 & & & & \ddots \\ & & & & & & [M_N] \end{bmatrix} \cdot \begin{bmatrix} a_0 \\ b_0 \\ a_1 \\ b_1 \\ a_2 \\ b_2 \\ \vdots \\ a_j \\ b_j \\ \vdots \\ a_N \\ b_N \end{bmatrix} = 0 \tag{16a}$$

where

$$M_0 = \omega\epsilon_0\left\{\frac{n_1^2 J_0'(\chi_1 a)}{\chi_1 J_0(\chi_1 a)} + \frac{n_c^2 k_0'(\chi_c a)}{\chi_c k_0(\chi_c a)}\right\} \tag{16b}$$

$$M_0' = \omega\mu_0\left\{\frac{J_0'(\chi_1 a)}{\chi_1 J_0(\chi_1 a)} + \frac{k_0'(\chi_c a)}{\chi_c k_0(\chi_c a)}\right\} \tag{16c}$$

and $[M_j]$ denotes the second-order square matrix whose determinant satisfies

$$\det[M_j] = k_0^2\left\{\frac{n_1^2 J_j'(\chi_1 a)}{\chi_1 J_j(\chi_1 a)} + \frac{n_c^2 k_j'(\chi_c a)}{\chi_c k_j(\chi_c a)}\right\} \cdot \left\{\frac{J_j'(\chi_1 a)}{\chi_1 J_j(\chi_1 a)} + \frac{k_j'(\chi_c a)}{\chi_c k_j(\chi_c a)}\right\} - \beta^2\left(\frac{j}{a}\right)^2\left(\frac{1}{\chi_1^2}+\frac{1}{\chi_c^2}\right)^2. \tag{16d}$$

Hence the eigenvalue equation (12) can be expressed as

$$M_0 \cdot M_0' \cdot \prod_{j=1}^{N} \det[M_j] = 0 \tag{17}$$

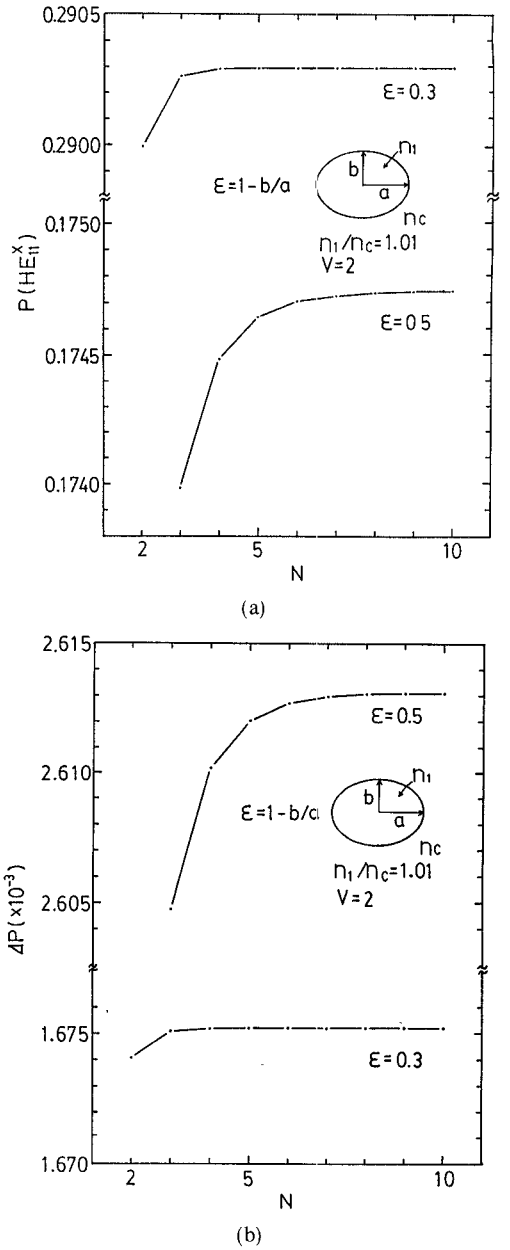

Fig. 4. Convergence characteristics of calculated propagation constants for elliptical core. (a) P value of HE_{11}^{y} mode. (b) ΔP, i.e., the difference between the P values for the HE_{11}^{y} and HE_{11}^{x} modes.

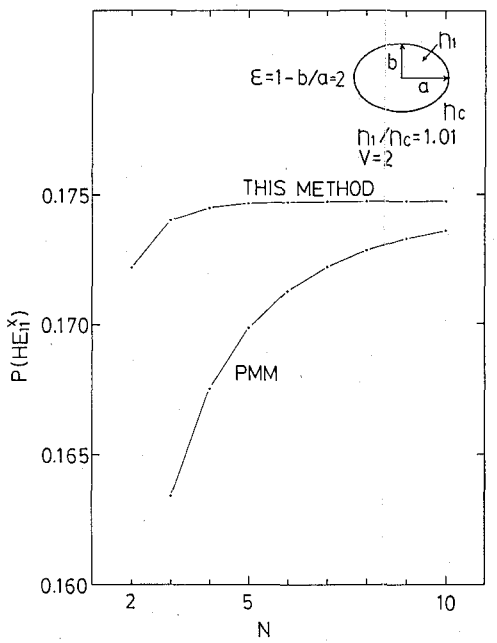

Fig. 5. Comparison of convergence of the P value for the HE_{11}^{y} mode with the point-matching method [10].

leading to three types of relations:

$$M_0 = 0 \qquad M_0' = 0 \quad \text{and} \quad \det\left[M_j\right] = 0.$$

It is known in optical fiber theory [9] that these solutions correspond to TM modes, TE modes, and hybrid modes, respectively.

Thus, the eigenvalue equations of a circular step-index optical fiber can be derived from the general formulation in the previous section, and the latter has been proved.

V. Analysis of Elliptical-Core Fibers

In this section, numerical analyses of step-index optical fibers having an elliptical core are presented.

We define three parameters: ellipticity ϵ, normalized wavenumber V, and normalized propagation constant P, as

$$\epsilon = 1 - b/a \tag{18a}$$

$$V = k_0 a \sqrt{n_1^2 - n_C^2} \tag{18b}$$

$$P = \frac{(\beta/k_0)^2 - n_C^2}{n_1^2 - n_C^2} \tag{18c}$$

where a and b are the major and minor axes of the elliptical core, respectively.

The designation of modes is given according to those in circular step-index fibers. The subscripts x and y denote the polarization axes in the HE_{11} modes.

Fig. 4(a) shows how the calculated P value converges as N, the number of terms of the Fourier expansion of the field variables, increases. Here N denotes the number of terms for E or H; the total number is therefore $2N$. Fig. 4(b) shows the convergence of ΔP, i.e., the difference between the P values for the HE_{11}^{y} and HE_{11}^{x} modes.

Fig. 5 shows a comparison of the convergence for the HE_{11}^{y} mode with that in the point-matching method (PMM)

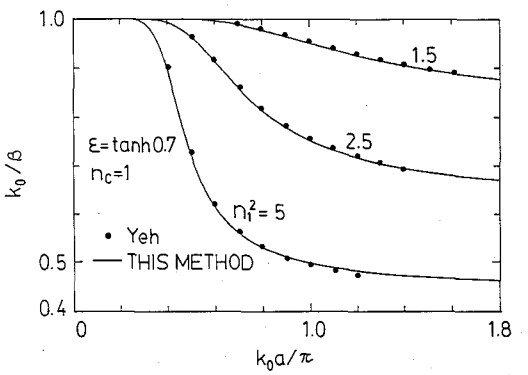

Fig. 6. Comparison of the propagation characteristics for large index differences with Yeh's analytical solutions [8] for elliptical core.

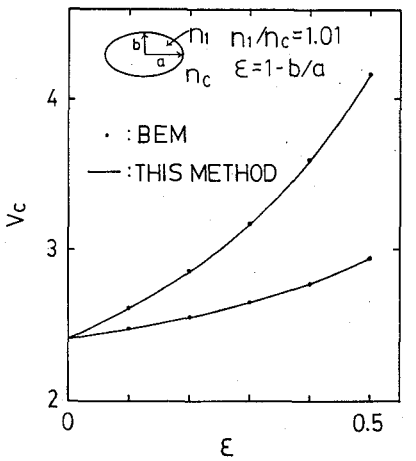

Fig. 7. Normalized cutoff frequencies V_c of the TE_{01} and HE_{21} modes as a function of the ellipticity ϵ. The solid curves show the results of this method; the dots show the results of conventional BEM [5].

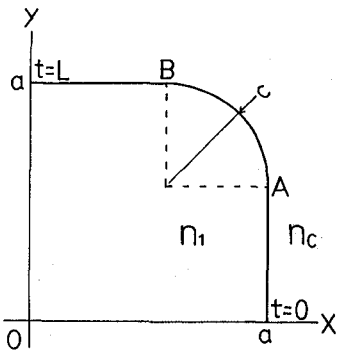

Fig. 8. Cross section of the rectangular core. The corner is rounded to investigate the effect of its radius of curvature c.

using a circular-harmonics expansion [10]. It is found that convergence in this method is much faster than in the point-matching method.

So far, the index difference between the core and cladding is assumed to be 1 percent. However, it is desirable to show the results for higher index differences to demonstrate the validity of the proposed vectorial wave analysis. Fig. 6 compares the computed propagation characteristics for large index differences with Yeh's analytical solutions [8]. The two solutions show good agreement.

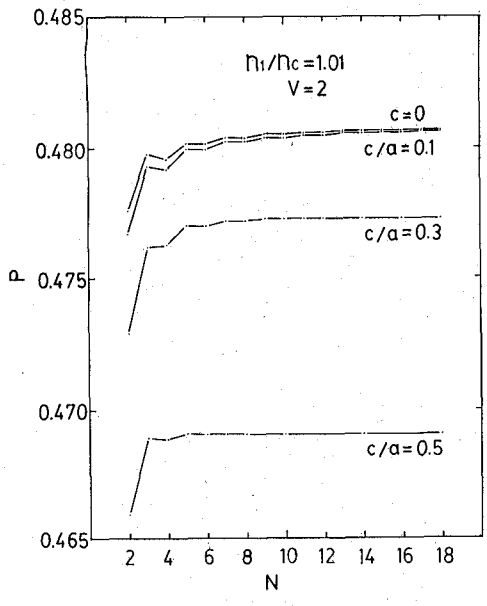

Fig. 9. Convergence of P value for the HE_{11} mode for rectangular cores.

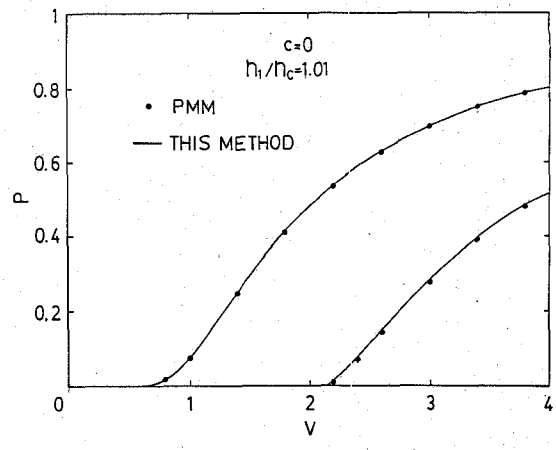

Fig. 10. Propagation characteristics of the dominant (HE_{11}) mode and the first higher order (TE_{01}) mode, for the truly rectangular shape ($c = 0$). The numerical analysis of the point-matching method (PMM) [11] is shown in dots.

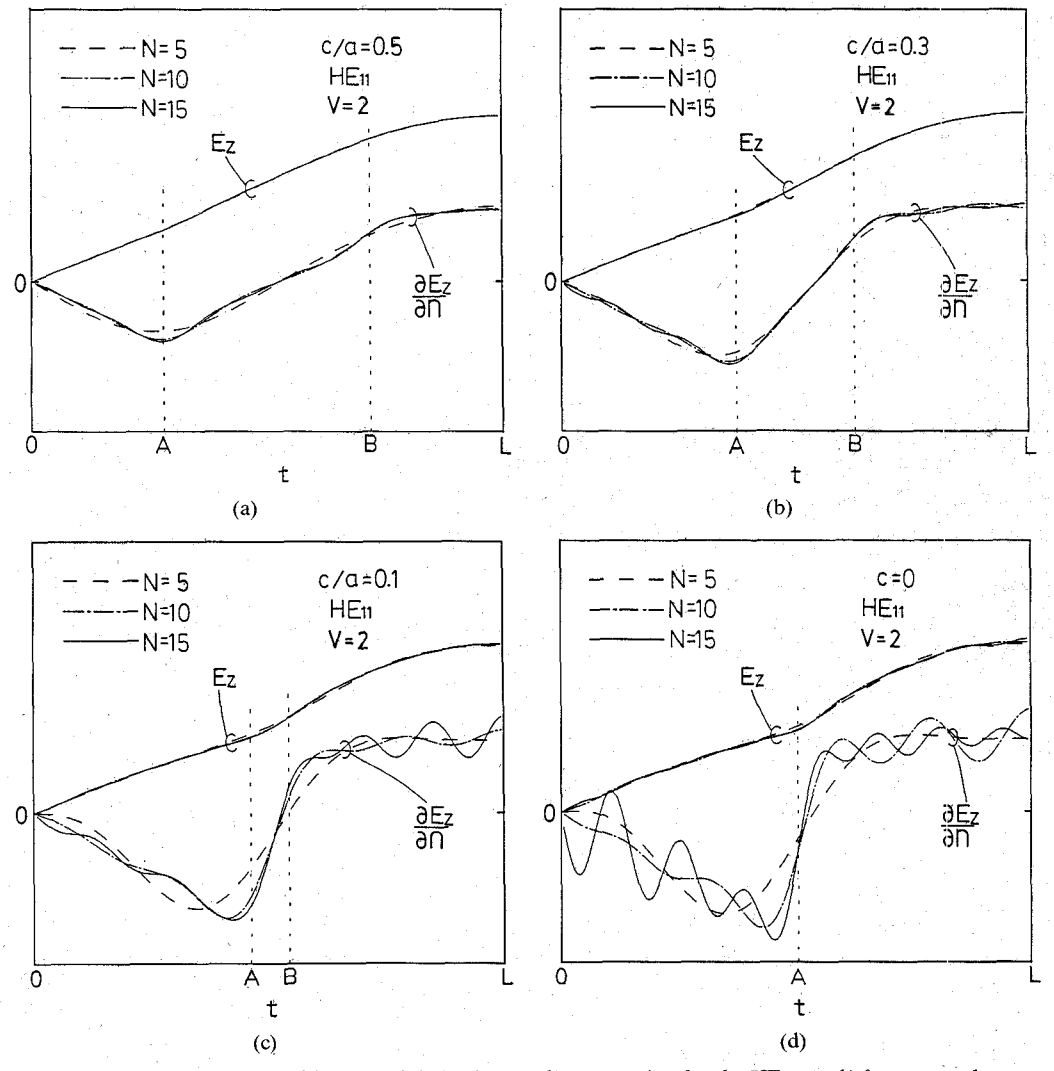

Fig. 11. Calculated electric field and its normal derivatives to the core region for the HE_{11} mode for rectangular cores with the number of Fourier expansion of field variables N increased. (a) $c/a = 0.5$. (b) $c/a = 0.3$. (c) $c/a = 0.1$. (d) $c = 0$.

Some calculated results for higher order modes are shown in Fig. 7. In this figure, the normalized cutoff frequencies V_c of the first and second higher order modes are shown as functions of the ellipticity ϵ. The solid curves (results of this method) and the dots (results of the conventional BEM [5]) show good agreement.

VI. Analysis of Rectangular Dielectric Waveguides

In the present analyses, the field variables on the boundary are Fourier-expanded on the curvilinear coordinate as described in Section III. Such a formulation does not present a problem if the boundary is perfectly smooth. However, when corners exist on the boundary, the normal and tangential derivatives of the electromagnetic fields become discontinuous, whereas the Fourier series is continuous and could be differentiated. This discrepancy results in a reduction of the numerical accuracy.

In this section, we present numerical analyses of rectangular dielectric waveguides to investigate the effect of the boundary shape on the numerical accuracy. Fig. 8 shows the cross section of a rectangular core. The corner is rounded to investigate the effect of its radius of curvature c; for a truly rectangular shape $c = 0$.

Fig. 9 shows the convergence of P for the HE_{11} mode. As c/a is decreased, i.e., as the rectangular corner becomes sharper, the convergence becomes slower, but not drastically.

The solid curves in Fig. 10 show the propagation characteristics of the dominant (HE_{11}) and the first higher order (TE_{01}) modes for the truly rectangular shape ($c = 0$). The results of the point-matching analysis [11] are shown by dots for comparison. The results of the two methods are in good agreement.

We can also calculate the electromagnetic fields using (10) and (11) after solving (12). Figs. 11 and 12 show the calculated electric field and its normal derivatives on the boundary for the HE_{11} and TE_{01} modes, respectively. In these figures, "A" and "B" on the abscissa indicate the ends of the curved portion. As the number of Fourier expansion terms N increases, the electric field on the boundary converges, whereas the normal derivative has ripples whose amplitudes become larger as the radius of curvature c decreases.

VII. Discussion

1) The proposed method is simpler than the conventional BEM because of the absence of singularities in the integration. It is also simpler than the extended boundary condition method because (5) is applied directly to the z components of the electromagnetic fields, and only the boundary values of these field variables are used as unknown variables.

2) In this formulation, electromagnetic fields on the boundary are expanded in Fourier series. In comparison with the conventional BEM analyses, the application of the boundary condition becomes much easier. It can be made only by equating term by term the Fourier spatial frequency components of the tangential field on both sides of the boundary.

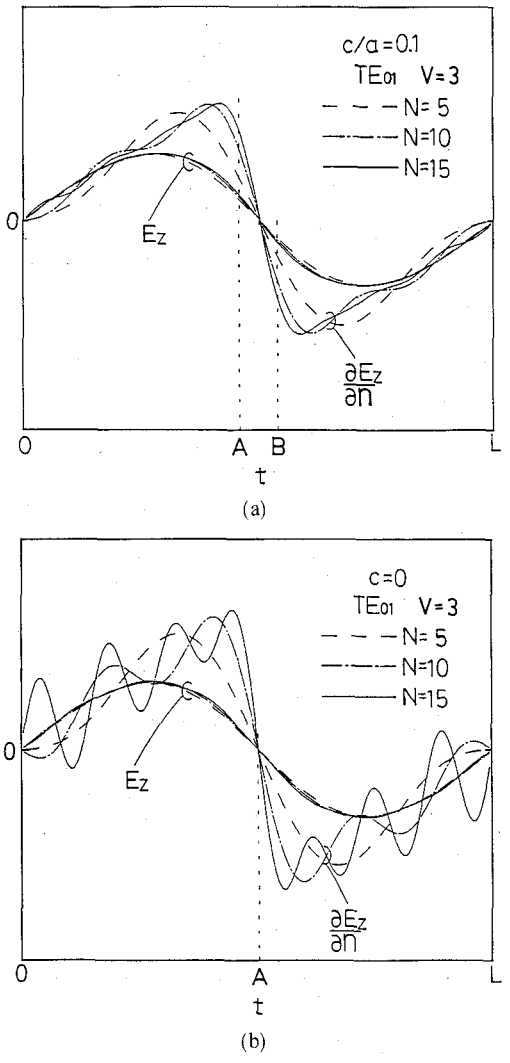

Fig. 12. Same as in Fig. 11 for TE_{01} modes. (a) $c/a = 0.1$ (b) $c = 0$.

3) In the derivation of eigenvalue equations of the circular step-index optical fiber, a rigorous eigenvalue equation has been obtained without any spurious solutions. In actual numerical analyses, we have never encountered any spurious solutions.

4) Figs. 4 and 9 indicate that the convergence is very fast regardless of the boundary shape. The calculation results have been proved to be correct through comparison with those by other numerical analyses, as shown in Figs. 5, 6, 7, and 10.

VIII. Conclusion

Vectorial wave analyses of optical fibers having arbitrarily shaped uniform cores have been carried out by the boundary integral method without using Green's function. Both the simplicity and the usefulness of the new method have been demonstrated. The accuracy of the calculated propagation constants is high even when corners exist on the boundary.

REFERENCES

[1] N. Kishi and T. Okoshi, "Proposal for a boundary-integral method without using Green's function," *IEEE Trans. Microwave Theory Tech.*, vol. MTT-35, pp. 887–892, Oct. 1987.

[2] T. Okoshi and T. Miyoshi, "The planar circuit—An approach to microwave integrated circuitry," *IEEE Trans. Microwave Theory Tech.*, vol. MTT-20, pp. 245–252, Apr. 1972.

[3] C. A. Brebbia, *Boundary Element Method for Engineers*. London: Pentech Press, 1978.

[4] S. Kagami and I. Fukai, "Application of boundary-element method to electromagnetic field problems," *IEEE Trans. Microwave Theory Tech.*, vol. MTT-32, pp. 455–461, Apr. 1984.

[5] M. Matsubara, "Boundary element analysis of polarization holding fibers," *Trans. IECE Japan*, vol. J67-B, pp. 968–973, Sept. 1984 (in Japanese).

[6] R. H. T. Bates, "Analytic constraints on electromagnetic field computations," *IEEE Trans. Microwave Theory Tech.*, vol. MTT-23, pp. 605–623, Aug. 1975.

[7] N. Morita, "A method extending the boundary conditions for analyzing guided modes of dielectric waveguides of arbitrary cross-sectional shape," *IEEE Trans. Microwave Theory Tech.*, vol. MTT-30, pp. 6–12, Jan. 1982.

[8] C. Yeh, "Elliptical dielectric waveguides," *J. Appl. Phys.*, vol. 33, pp. 3235–3243, Nov. 1962.

[9] T. Okoshi, *Optical Fibers*. New York: Academic Press, 1982.

[10] E. Yamashita, K. Atsuki, O. Hashimoto, and K. Kamijo, "Modal analysis of homogeneous optical fibers with deformed boundaries," *IEEE Trans. Microwave Theory Tech.*, vol. MTT-32, pp. 455–461, Apr. 1984.

[11] J. E. Goell, "A circular-harmonic computer analysis of rectangular dielectric waveguides," *Bell Syst. Tech. J.*, vol. 51, pp. 2133–2160, Sept. 1969.

✠

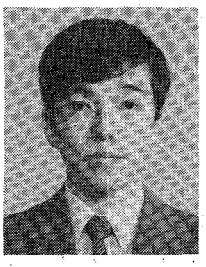

Naoto Kishi (S'85–M'87) was born in Tokyo, Japan, on March 11, 1960. He received the B.S. and M.S. degrees from the University of Electro-Communications, Tokyo, Japan, in 1982 and 1984, respectively, and the Ph.D. degree from the University of Tokyo, Tokyo, Japan, in 1987, all in electrical engineering.

He became a Research Associate in the Department of Electronic Engineering at the University of Electro-Communications in 1987. His main fields of interest are microwave and lightwave circuits and transmission lines of various types, numerical analysis methods of electromagnetic fields, and musical instruments.

Dr. Kishi is a member of the Institute of Electronics, Informations and Communication Engineers of Japan.

✠

Takanori Okoshi (S'56–M'60–SM'81–F'83) was born in Tokyo, Japan, on September 16, 1932. He received the B.S., M.S., and Ph.D. degrees from the University of Tokyo, Tokyo, Japan, in 1955, 1957, and 1960, respectively, all in electrical engineering.

In 1960 he was appointed Instructor and in 1961 Associate Professor in the Department of Electronic Engineering, University of Tokyo. From 1963 through 1964, while on leave from the University of Tokyo, he was with Bell Laboratories, Murray Hill, NJ, where he was engaged in research on electron guns. In January 1977 he became a Professor at the University of Tokyo. In 1987 he was elected to the position of Founding Director of the Research Center for Advanced Science and Technology (RCAST), a newly established research institute at the University of Tokyo. At present Dr. Okoshi is also a Guest Research Fellow of the Communications Research Laboratory of the Japanese Government, Commission-D Chairman of URSI (International Union of Radio Science), and President of the Japanese Committee for URSI.

The main fields of Dr. Okoshi's present interest are optical fiber communications and measurements, in particular, coherent optical fiber communications and photon-counting optical measurements. He has written 15 books, including four in English: *Three-Dimensional Imaging Techniques* (Academic Press, 1976), *Optical Fibers* (Academic Press, 1982), *Planar Circuits* (Springer, 1984), and *Coherent Optical Fiber Communications* (KTK/Kluwer, 1988, with Dr. K. Kikuchi). Dr. Okoshi has been awarded 15 prizes from four academic institutions, including the IEEE. He holds 15 Japanese patents and five U.S. patents.